View metadata, citation and similar papers at core.ac.uk

brought to you by CORE

provided by Kent Academic Repository

# Kent Academic Repository

## Full text document (pdf)

### Citation for published version

Mulligan, Christopher and Fenollar-Ferrer, Cristina and Fitzgerald, Gabriel A and Vergara-Jaque, Ariela and Kaufmann, Desirée and Li, Yan and Forrest, Lucy R and Mindell, Joseph A (2016) The bacterial dicarboxylate transporter VcINDY uses a two-domain elevator-type mechanism. Nature structural & molecular biology, 23 (3). pp. 256-263. ISSN 1545-9985.

### DOI

https://doi.org/10.1038/nsmb.3166

### Link to record in KAR

http://kar.kent.ac.uk/61674/

### Document Version

Author's Accepted Manuscript

**Copyright & reuse**

Content in the Kent Academic Repository is made available for research purposes. Unless otherwise stated all content is protected by copyright and in the absence of an open licence (eg Creative Commons), permissions for further reuse of content should be sought from the publisher, author or other copyright holder.

**Versions of research**

The version in the Kent Academic Repository may differ from the final published version.
Users are advised to check **http://kar.kent.ac.uk** for the status of the paper. **Users should always cite the published version of record.**

**Enquiries**

For any further enquiries regarding the licence status of this document, please contact:
**researchsupport@kent.ac.uk**

If you believe this document infringes copyright then please contact the KAR admin team with the take-down information provided at **http://kar.kent.ac.uk/contact.html**

KAR Kent Academic Repository

University of Kent

**The bacterial dicarboxylate transporter, VcINDY, uses a two-domain elevator-type mechanism**

Christopher Mulligan[1], Cristina Fenollar-Ferrer[2,4], Gabriel A. Fitzgerald[1], Ariela Vergara-Jaque[2], Desirée Kaufmann[4,5], Yan Li[3], Lucy R. Forrest[2,4]*, Joseph A. Mindell[1]*

[1]Membrane Transport Biophysics Section, [2]Computational Structural Biology Unit, and [3]Protein/Peptide Sequencing Facility, Porter Neuroscience Research Center, National Institute of Neurological Disorders and Stroke, National Institutes of Health, Bethesda, MD 20892. [4]Max Planck Institute of Biophysics, Frankfurt am Main, Germany. [5]Present address: Institute of Molecular Biology, Mainz, Germany.

*To whom correspondence should be addressed: Lucy R. Forrest (lucy.forrest@nih.gov) and Joseph A. Mindell (mindellj@ninds.nih.gov).

**Abbreviations**

TM, transmembrane; HP, helical hairpin; DASS, divalent anion sodium symporter; dicarboxylate/amino acid:cation symporters, DAACS; TCDB, transporter classification database; PDB, protein data bank; SEC (size exclusion chromatography);

**Acknowledgements**

We thank Anirban Banerjee for helpful discussions and Merritt Maduke, Jose Faraldo-Gomez, Gary Rudnick, and Mark Mayer for critical reviews of the manuscript. Ariela Vergara-Jaque is recipient of the L'Oreal Chile-UNESCO Women in Science Fellowship and the L'Oreal-UNESCO Rising Talent Award. This work was supported by the Division of Intramural Research of the NIH, National Institute of Neurological Disorders and Stroke.

**Abstract**

Secondary transporters use alternating access mechanisms to couple uphill substrate movement to downhill flux of a coupling ion, presenting binding sites alternately to either side of the membrane. Most known transporters utilize a "rocking bundle" motion, where the protein moves around an immobile substrate binding site to regulate ingress. However, one protein, the glutamate transporter homolog $Glt_{Ph}$ translocates its entire substrate binding site vertically across the width of the membrane, a so-called "elevator" mechanism. Here we examine an unrelated transporter, the $Na^+$/succinate transporter VcINDY. With the crystal structure of an inward facing state of VcINDY as a template, we used the "repeat swap" approach to computationally predict the structure of the outward-facing state of the transporter. Our model suggests that VcINDY undergoes a substantial elevator-like movement to transfer its substrate binding site, with a vertical translation of ~15 Å and a rotation of 43°. Crosslinks formed between three different pairs of introduced cysteine residues, proximate only in the outward-facing state, confirm this large-scale motion. These crosslinks completely inhibit transport, demonstrating that such movement is essential for transport. In contrast, multiple crosslinks across the VcINDY dimer interface preserve transport function, revealing an absence of large scale coupling between VcINDY protomers.

**Introduction**

Secondary active transporters constitute a large class of proteins responsible for catalyzing the passage of key compounds across the lipid bilayer in all living cells. These molecular machines harness the energy supplied by the electrochemical gradient of one solute, usually a coupling ion like $H^+$ or $Na^+$, to power the transport of another solute against its concentration gradient. Secondary transporters operate by an alternating access mechanism in which conformational changes in the protein alternately expose the substrate-binding site to either side of the membrane. A minimum of two conformational states are therefore required to achieve alternating access; an inward-facing state, where the substrate is accessible to the cytoplasmic side of the membrane only, and an outward-facing state, where the substrate is only accessible to the extracellular side[1,2]. Many transporters also utilize intermediate "occluded" states in which the substrate-binding site is accessible to neither side of the membrane[3,4].

The ever-growing collection of secondary transporter crystal structures reveals a remarkable diversity of protein folds; structural and functional investigations have begun to illuminate the conformational mechanisms by which these folds achieve alternating access. Of the 17 secondary transporter folds reported to date, the Major Facilitator Superfamily (MFS) fold and the LeuT fold represent a majority of the known protein sequences and an overwhelming majority of the known X-ray crystal structures[5,6]. In both cases, their conformational mechanisms involve movement of helices around a substrate binding site, which is usually situated at the center of the lipid bilayer. While the overall mechanism has been described as movements of domains in "rocking bundle" or "rocker-switch" type conformational changes, the available evidence also suggests a role for individual "gating" helices that help determine intermediate steps in the transport cycle[7-11]. Either way, for both of these large families, the substrate retains its relative position in the membrane regardless of the conformation of the transporter.

A dramatically different route to achieving alternating access involves an elevator-type (or "carrier") mechanism; here, the substrate-binding site itself is moved. Elevator-type transporters are composed of two domains; a scaffold domain that remains relatively rigid during the transport cycle, and

a second domain that contains all the residues necessary to bind the substrate, referred to as the transport domain. This mechanism derives its name from the elevator-like rigid body translation of the transport domain back and forth across the hydrophobic barrier provided by the protein and lipid bilayer by moving the entirety of the substrate-binding site and allowing the substrate to be alternately exposed to both sides of the membrane. To date, only the glutamate transporter homolog $Glt_{Ph}$ has been convincingly shown to employ an elevator mechanism[12,13]. $Glt_{Ph}$ belongs to a relatively small family of proteins (the dicarboxylate/amino acid:cation symporters, DAACS; transporter classification database (TCDB) family 2.A.23), raising the possibility that its mechanism is unique to this small family. However, a similar mechanism has recently been hypothesized for the $Na^+/H^+$ antiporters, though this proposal remains controversial[14]. Thus, the prevalence of elevator-like mechanisms in biology remains a compelling and unanswered puzzle.

Here, using structural modeling combined with extensive disulfide crosslinking, biochemical, and functional characterization of purified VcINDY, we report that the $Na^+$/succinate transporter VcINDY also employs an elevator-type mechanism. VcINDY, from *Vibrio cholerae*, belongs to the divalent anion sodium symporter (DASS) family of transporters (TDCB family 2.A.47), which also contains members of the SLC13 family responsible for the uptake of citrate, Krebs cycle intermediates, and sulfate, in humans[15-17]. VcINDY is the only DASS family member for which a high-resolution structure is known; this structure represents a unique fold in the Protein Databank[18]. The 3.2 Å structure of VcINDY reveals a dimeric architecture; the positioning of the bound ligand, in this case citrate, indicates that this structure reflects an inward-facing state of this transporter. Each protomer consists of 11 transmembrane (TM) helices that can be partitioned into two distinct domains; a scaffold domain that forms all inter-protomer contacts and a transport domain that houses the substrate binding site (Fig. 1 and 2) – an arrangement highly reminiscent of $Glt_{Ph}$.

The results presented here computationally predict and experimentally confirm an outward-facing state of VcINDY, and indicate that a ~15 Å translation accompanied by a 43° rigid body rotation of the transport domain occurs to expose the substrate binding site to the external solution. This work

therefore reveals a second transporter family, with a different fold than $Glt_{Ph}$, that employs an elevator-type mechanism with similarities to that of $Glt_{Ph}$, but also with key differences. Given the relationship between VcINDY and other families in the large "Ion Transporter (IT) Superfamily" we raise the possibility that this superfamily shares key features of the elevator mechanism and that, like the rocking bundle-type mechanisms, this conformational strategy is also widespread in secondary transport[19,20].

**Results**

VcINDY contains inverted-topology structural repeats

The only structural information available for VcINDY corresponds to the substrate-bound, inward-facing state of the transporter[18]. Transporters are exceedingly dynamic proteins that need to fluctuate between multiple conformational states to function; so, while informative, a structure of a single conformational state reveals very little about the actual mechanism of transport. We sought to explore additional conformations of VcINDY using computational modeling, taking advantage of pseudo-symmetrical repeats apparent from the crystal structure[18]. In this procedure, called repeat-swap homology modeling, we identify repeating structural units by careful analysis of the crystal structure; we then swap the conformations of these repeating units[21]. Underlying the success of this procedure is the fact that the structures of these repeating units are not perfectly symmetric; it is the subtle conformational differences between the repeating units that lead to the prediction of alternate conformational states upon interconversion. Repeat-swap homology modeling has been applied to several transporter families and found to produce accurate predictions of even dramatically different conformations[12,21-23].

VcINDY contains an, an inverted-topology structural repeat related by pseudo two-fold symmetry around the axis in the plane of the membrane[18]; repeat unit 1 (RU1) consisting of TM helices 2-6 (defined here as residues 42-242) and repeat unit 2 (RU2) consisting of TM helices 7-11 (residues 260-453; Fig. 1a and b, RU1: blue and cyan helices, RU2: red and orange helices). TM1 is a peripheral helix in VcINDY and is not part of either repeating unit. Our alignments of the amino acid sequences of RU1 and RU2 revealed

a low sequence identity of ~20% (Supplementary Fig. 1a). However, upon superimposition of the repeating units, we clearly see that they share a similar architecture, with a root mean square deviation (RMSD) value for the Cα atoms of ~4.3 Å when the whole repeat is superimposed (Fig. 1c). When we divided up the repeats so that we compared only the helices in each repeat comprising the transport domain (blue/red) or only the helices in each repeat comprising the scaffold domain (cyan/orange), we found much higher structural similarity (RMSD values of 2.0-2.1 Å). This result suggests that the main contribution to the structural differences between the repeats comes from the orientation of the transport domain helices relative to the scaffold domain helices (Fig. 1c). Repeating the comparisons using template modeling scores (TM-scores), which give a measure of structural similarity that is independent of segment length (values between 0 and 1; 1 being structurally identical), underscores this observation. Specifically, superimposing the entirety of each repeat gave a TM-score of 0.52, which increased to 0.78 and 0.83 when comparing only the transport and scaffold domain helices, respectively.

The inward-facing state structure of VcINDY can be used to predict an alternate conformation

We applied the repeat-swap procedure to VcINDY by modeling the conformation of RU1 using RU2 as a template, and vice versa (Supplementary Fig. S1b). The resulting model revealed a substantial conformational change compared to the inward-facing crystal structure (Fig. 2b). As a result of this conformational change, which is localized to the transport domain, the substrate binding site is exposed to the extracellular side of the membrane, clearly demonstrating that the repeat-swapped model represents a putative outward-facing state of VcINDY (Fig. 2c and Supplementary Fig. 2a and b).

To analyze the conformational changes that occur during the transformation from the inward- to the outward-facing conformation, we superimposed the model onto the structure using only helices from the oligomerization interface, which also allowed us to construct a model of the dimer (Fig. 2b). We note that this model is therefore based on the assumption that the dimer interface is unchanged during transport (an assumption we test explicitly below). This comparison predicts that the entire transport domain would undergo a ~15 Å vertical translation accompanied by a 43° rotation (Supplementary Fig.

S2a). As a consequence, transport domain residues would be displaced by 10-20 Å (Supplementary Fig. S2b).

Design of site-specific cysteine pairs to test the outward-facing model

A key prediction of the outward-facing repeat-swapped model is that transport requires a major translocation of the transport domain across the membrane, accompanied by a significant rotation. If such a motion indeed occurs, then there should be residues that are far apart in one state, but that are brought into close proximity in the other state. To test this idea, we introduced pairs of cysteine residues at positions that are widely separated in the inward-facing structure (Cβ-Cβ distance >12 Å), but are brought closely enough together (Cβ-Cβ distance <7 Å) in the predicted outward-facing state that they could potentially form disulfide links. The ready formation of crosslinks in these proteins would strongly support the proposed conformational change. We also predict that, by confining the protein to a single state in the transport cycle, these crosslinks should strongly inhibit transport. To validate this approach, we also designed a cysteine pair that should selectively stabilize the known inward-facing state by substituting residues that are distant in the outward-facing model, but in close proximity in the inward-facing crystal structure.

As a starting construct for our experiments we used a mutant in which we substituted serine residues for the three native cysteines in VcINDY, giving us a cysteine-free background (Cysless), which is stable and, aside from having a ~4-fold lower transport rate (Supplementary Fig. 3a), is functionally equivalent to wild type VcINDY at catalyzing $Na^+$-driven succinate uptake.

In total, we introduced 24 different combinations of double cysteine mutants into the interface between the transport and scaffold domains. However, most of these mutant combinations resulted in unstable protein that expressed poorly or aggregated (data not shown). The majority of these cysteine substitutions were located towards the center of the transport domain in positions with low solvent accessibility. Only one of the "buried" interfacial pairs that we tested, T154C/V272C, yielded stable protein and was used in further studies (Fig. 2b). The distance between the Cβ-Cβ atoms of T154 (from

HP1) and V272 (from TM7) in the inward-facing structure ($d_{ifs}$) = 18.7 Å, whereas in the outward-facing model the distance ($d_{ofm}$) = 3.9 Å. We subsequently targeted regions at the periphery of the interface, in particular the symmetry related helices 4c and 9c. Solvent accessible loops were more tolerant to modification so we were able to introduce two cysteine pairs, A120C/V165C in helix 4c/HP1 ($d_{ifs}$ = 11.7 Å; $d_{ofm}$ = 4.7 Å), and A346C/V364C in helix 9c/HP2 ($d_{ifs}$ = 16 Å; $d_{ofm}$ = 5.6 Å), with no apparent reduction in protein stability (Fig. 2b). Together, these cysteine pairs occupy three different positions at the interface between the transport and scaffold domains, providing good coverage of the conformational change predicted by our model. To stabilize the inward-facing state, we introduced the double cysteine mutant L60C/S381C in TM2/HP2 ($d_{ifs}$ = 6.9 Å; $d_{ofs}$ = 20.6 Å, Supplementary Fig. 5a). All four cysteine pairs were well tolerated by VcINDY under reducing conditions, as each purified mutant produced a single symmetrical peak upon size exclusion chromatography (SEC), and demonstrated robust transport activity (Supplementary Fig. 3b).

Cysteine crosslinking supports the outward-facing model

In some experiments we generated crosslinks using $HgCl_2$, which can act as a homobifunctional crosslinking reagent, in others we used oxidizing agent copper phenanthroline (CuPhen) to catalyze disulfide bond formation. We screened for successful crosslinks using the gel-shift assay described by Basilio et al[24]. Specifically, after treatment with crosslinking reagent, we enumerated the remaining free cysteines by treating the protein with a 5 kDa PEG-maleimide (mPEG5K), which causes a substantial shift in the protein's gel mobility upon reaction with free cysteine. If the introduced cysteines are crosslinked with each other, however, then they will be unable to react with mPEG5K and the protein band will run as monomeric VcINDY on SDS-PAGE. Before crosslinking, each double cysteine mutant was almost completely PEGylated after incubation with mPEG5K, demonstrating that both cysteines in each mutant were accessible to the probe (Fig. 3 and Supplementary Fig. 5b). In contrast, after treatment with $HgCl_2$ or CuPhen all three outward-stabilizing double cysteine mutants and the single inward-stabilizing mutant were completely protected from PEGylation (Fig. 3 and Supplementary Fig. 4, 5b), suggesting

that all four cysteine pairs successfully formed intramolecular crosslinks. Treatment of the double cysteine mutants with crosslinking reagents did not significantly affect the elution volume of the protein peak on SEC, but did result in slight peak broadening; we observed minimal aggregation for these proteins (data not shown). These results indicate that treatment with crosslinking reagent is well tolerated and that the fold of the crosslinked protein is not disrupted.

To obtain direct physical evidence of crosslink formation we analyzed the double cysteine mutants using liquid chromatography-tandem mass spectrometry (LC-MS/MS, Fig. 4). If we indeed formed crosslinks in the cysteine mutants then we should be able to directly detect the crosslinked peptides using this approach. For these experiments we used only CuPhen to crosslink because of concerns about adding the toxic metal $Hg^{2+}$ to the Mass Spectrometer and because of uncertainty regarding whether $Hg^{2+}$-mediated crosslinks contain a metal bridge or only a disulfide[24]. After incubating the cysteine mutants with either CuPhen or DTT (to prevent spontaneous crosslink formation) we digested the proteins, separated the proteolytic fragments by liquid chromatography, and Mass Spec, unambiguously assigning all the peptides produced (Fig. 4). Upon interrogation of the LC-MS/MS output for specific peptides we identified disulfide-crosslinked peptides in the CuPhen-treated samples of both A120C/V165C and T154C/V272C; these peptides were completely absent in the reduced protein samples (Fig. 4a and b, right panel). We also obtained LC-MS/MS data consistent with crosslink formation between A346C and V364C. However, an insufficient number of proteolytic sites between residues 360 and 390 prevented us from confidently assigning the MS fragment peaks (data not shown). Due to this technical limitation, we were also unable to obtain consistent LC-MS/MS data for the inward-stabilizing mutant L60C/S381C. These data unequivocally demonstrate crosslink formation between two of the introduced cysteine pairs, and strongly suggest that the mPEG5K labeling results for the other two pairs indeed reflect crosslink formation. Formation of these crosslinks strongly supports our prediction that the outward facing conformation of VcINDY requires a specific, large excursion of the transport domain. (Supplementary Movie 2).

Crosslinking VcINDY abolishes transport activity

Our hypothesis for the VcINDY transport mechanism, based on the model of the outward-facing conformation, is that the translocation of the transport domain is essential for transport, physically moving the binding site from one side of the membrane to the other (Fig. 2 and Supplementary Movie 1). If true, then crosslinking VcINDY in either the inward- or outward-facing state should straightjacket the transporter and curtail its transport activity. We tested this prediction by reconstituting the double cysteine mutants into proteoliposomes and measuring succinate transport activity in the presence and absence of a disulfide link (Fig. 5). Indeed, when we form crosslinks by treating proteoliposomes containing double cysteine mutants with excess $HgCl_2$ (on both sides of the membrane) we observed almost complete cessation of succinate transport activity for all three outward-stabilizing double cysteine mutants (Fig. 5). Transport activity was almost completely restored when the crosslinks were broken by subsequently treating proteoliposomes with 1 mM DTT after $HgCl_2$ removal (again, on both sides of the membrane), indicating that the abolition of transport was caused by disulfide bond formation. In addition, recovery of full transport activity demonstrates that $HgCl_2$ treatment does not irreversibly damage the protein or the lipid bilayer. Similarly, crosslinking the reconstituted inward-stabilizing mutant also reversibly abolished transport activity (Supplementary Fig. 5c). Crosslinking the purified mutant proteins prior to reconstitution also led to full inhibition of transport, as did CuPhen-mediated crosslinking, demonstrating the robustness of crosslink formation (data not shown). Cysless VcINDY retained the bulk of its transport activity (~60%) upon treatment with crosslinking reagent, again fully reversible on reduction (Fig. 5). This minor activity loss suggests, as others have reported for different transporters[24], that $HgCl_2$ can either interact with the protein in positions other than the cysteine residues or that the crosslinking reagent interacts with the lipid bilayer and compromises its integrity. In our case, however, the retention of substantial transport activity in the $HgCl_2$-treated Cysless protein confirms that the strong inhibition in the crosslinked proteins is due to the specific effects of the crosslinking agents on the double cysteine mutants. Together these results strongly support our

hypothesis that the large conformational change required to form the crosslinks is also an essential component of the transport process.

The dimer interface remains relatively rigid during transport

The data described so far demonstrate large-scale conformational changes between helices in the scaffold and helices in the transport domain. In constructing a model of the outward-facing dimer, as described above, we made the assumption that the helices contributing to the oligomerization interface (i.e., from the scaffold), would remain fixed relative to one another. We tested this assumption by assessing the functional effects of "stapling" the protomers together at several inter-protomer contact points. Thus, if substantial conformational changes at the dimer interface are essential for transport then stapling the protein at these positions should abolish transport activity.

According to the inward-facing crystal structure, the VcINDY dimer contains four inter-protomer contact points: TM helices 8 and 4b from one protomer interact with TM helix 3 and interfacial helix 4a from the other protomer, respectively; and helix 4a and TM helix 9b in one protomer interact with their counterparts in the other protomer (Fig. 6a). We introduced cysteine pairs into the dimer interface at these 4 contact points; Q86C (helix 4a)/S95C (TM4b), V68C (TM3)/S304C (TM8), N90C (helix 4a), and K316C (TM9). Due to the two-fold symmetry of the VcINDY homodimer, we expected the mutants containing two cysteine residues per protomer to form two disulfide bonds across the interface, whereas we expected the corresponding single cysteine mutants to form single disulfide bonds (with their symmetry-related counterparts). Each interfacial cysteine mutant was stable and exhibited robust transport activity when reconstituted into liposomes (Fig. 6 and Supplementary Fig. 6).

The inter-protomer crosslinks formed readily upon incubation with CuPhen, which we assessed by running the proteins on non-reducing SDS-PAGE gels; a shift of the protein band from the monomeric VcINDY molecular weight to that expected for the dimer indicates crosslinks formation (Fig. 6b, "D"). Purifying and then maintaining the mutants in reducing conditions completely prevented crosslink formation (Fig. 6b). Importantly for our functional assays, crosslinks remain stable during reconstitution

of the treated protein into liposomes, as ascertained by Western blot analysis (Fig. 6b "PL"). Incubation with 10 μM 2:1 CuPhen for 45 minutes at room temperature fully crosslinked all proteins except for the V68C/S304C mutant. V68C/S304C required 500 μM CuPhen to attain full crosslinking, which presumably reflects reduced accessibility of these residues to the crosslinking agent or sub-optimal alignment of the two cysteines.

We evaluated the transport competence of the crosslinked proteins by measuring $Na^+$-driven succinate uptake (Fig. 6c). All four "stapled" mutants exhibited robust transport activity after crosslink formation, demonstrating that there are no substantial conformational changes in these positions that are essential for transport (Fig. 6c). However, upon closer analysis, the functional effects of stapling the dimer interface varied depending on the position of the disulfide crosslink. Crosslinking two of the mutants, V68C/S304C and N90C, had no discernable effect on their transport activity beyond the non-specific effects we observed for Cysless (Fig. 6c). Interestingly, however, crosslinking the other two mutants, Q86C/S95C and K316C, resulted in a 5-fold and 2-fold transport activity decrease, respectively. It is difficult to delineate from our current data why constraining the protein in these positions causes this inhibition. One possibility is that the cross-linking causes a local distortion in the scaffold domain that reduces the ability of the transport domain to move along it. Nevertheless, unlike the crosslinks between scaffold and transport domain, all of these crosslinks preserve at least partial transport activity. Further studies will be necessary to illuminate the underlying causes of these more subtle effects. As we found with $HgCl_2$, treating cysteine-free VcINDY with 0.5 mM CuPhen reduced the activity to ~60% compared to the untreated sample. In contrast, we observed no change in activity for Cysless upon treatment with 10 μM CuPhen (Fig. 6c). Cysteine-independent effects of CuPhen have been observed previously with proteoliposomes and membrane vesicles and have been attributed to $Cu^{2+}$ binding tightly to the membrane or the oxidizing environment reducing the integrity of the bilayer[25].

**Discussion**

In this study, we present a structural model of the outward-facing state of VcINDY along with extensive experimental data supporting this model. This work demonstrates that VcINDY utilizes an elevator-type movement, with protein excursions on the order of ~15 Å, that is an essential step in the transport cycle. Our conclusions are based on the formation of disulfide crosslinks between cysteine pairs introduced in three different locations, each physically separated in the inward-facing structure, but predicted by our model to be juxtaposed in the outward-facing state. That these crosslinks form readily shows that the protein can adopt the predicted outward-facing conformation; that they profoundly disrupt transport confirms that movement to and from this state is essential for transport. Moreover, preservation of transport activity in the presence of crosslinks across the dimer interface reveals that no major conformational change in this region is required for transport.

*Repeat-swap modeling provides access to structures not otherwise available*

Due to the dynamic nature of secondary transport, our understanding of their mechanism requires knowledge of multiple conformational states during the transport cycle. To obtain alternate conformations at useful resolutions, X-ray crystallography is the usual method of choice, although often results in the same conformation being trapped despite significant efforts to obtain different states. In this study, we demonstrate the power of an elegant modeling approach, based on the internal asymmetry found in the known structure of VcINDY, to predict alternate protein conformations, combined with extensive experimental evaluation. Internal asymmetry has been used to predict alternate conformations of members of several different transporter families, demonstrating that proteins with inverted-topology repeats conform to a strategy of asymmetry exchange, and providing testable, atomistic models for several different proteins with distinct folds[12,21,22]. Approximately three-quarters of all secondary transporters contain such internal symmetry, making this approach a viable option in the pursuit of mechanistic understanding on a broad scale[26].

As repeat-swap modeling is, in essence, a homology modeling technique, the error of the model depends on the difference in the sequences of the two repeats, which in the case of VcINDY is ~20%,

implying a structural error of 1-3 Å in the Cα positions[27]. However, our updated protocol reduces this error significantly, by including a second refinement step that effectively maintains the integrity of the domains moving relative to one another, while preserving the overall movement of those domains (see Methods; Supplementary Figs. 2 and 7). Overall this new strategy, and the success of the method on previous occasions, gives confidence that the overall conformational change predicted will be correct.

Comparison of the inward-facing state captured in the crystal structure of VcINDY with our outward-facing model, suggests that the transport domain moves vertically ~15 Å and rotates 43°, thereby translocating the substrate binding site to the other side of the hydrophobic barrier provided by TM helices 4 and 9. The extent to which the degree of this conformational change is representative of the true mechanism depends on the known structure. If the excursion of the transport domain in the template is large, i.e., because the asymmetry between the repeats is significant, then the excursion of the transport domain in the model will be equivalently large; as a consequence, the comparison between the model and structure will predict a more substantial conformational change. Insofar, though, as the X-ray structure of VcINDY accurately represents the inward-facing state (despite being bound to an inhibitor[18] rather than a transported substrate), the model should also represent the outward-facing state. The success of our experimental test of the model, with multiple successful crosslinks representing the outward-facing state, strongly suggests that the modeled conformation represents a native state, and that the conformational change is truly elevator-like.

*The crosslinked protein represents a native conformation of VcINDY*

A key assumption underlying our results is that the states stabilized by our crosslinks represent well-populated conformations accessible to the native protein rather than rarely-visited grotesques that have been kinetically trapped by the disulfide bond. We report crosslinks between three different cysteine pairs, distributed across the transport/scaffold domain interface. This combination of appositions would be extraordinarily difficult to achieve with a fundamentally different conformational change. Moreover, the wide range of conditions used in these experiments, including crosslink

formation using either CuPhen or $HgCl_2$ with protein in either detergent or lipid membranes, argues that we are sampling a native state of the protein. In addition, the consistent mobility of the crosslinked protein on size exclusion chromatography rules out the possibility of a reversibly denatured form of the protein that is stabilized by the crosslink.

The work described here was made more difficult by the sensitivity of VcINDY to modification, particularly at the interface between the transport domain and the scaffold domain. Single point mutations were sufficient to completely destabilize the protein. This apparent sensitivity is in stark contrast to the situation with $Glt_{Ph}$, which tolerated extensive modification. Is there an obvious reason for this difference in sensitivity? Comparison of the interfaces of the two proteins demonstrates that the surface of the transport domain that is predicted to slide against the scaffold domain in VcINDY contains 70% apolar amino acids; this patch of hydrophobic residues is significantly larger than in $Glt_{Ph}$, where only 46% of the residues are apolar. The additional hydrophobicity in the interface may not have tolerated oxidized cysteine.

*Other Transporters with Proposed Elevator-Type Mechanisms*

How does the movement of VcINDY compare with other proposed elevator-type transporters? Currently, the only transporter that can indisputably be called an elevator-type transporter is the glutamate transporter homolog, $Glt_{Ph}$[13,28]. Our results demonstrate that the transport domain of VcINDY undergoes a similar perpendicular and rotational movement to that of $Glt_{Ph}$ (~15 Å and 43° for VcINDY vs. 16 Å and 37° for $Glt_{Ph}$)[13].

Recently, it has been suggested that members of the cation-proton antiporter (CPA) family, exemplified by the $Na^+/H^+$ exchanger NhaA, employ an elevator-type mechanism, although this remains controversial. The CPA fold consists of a transport domain containing two unwound helices that cross in the middle of the membrane to form substrate binding sites. An experimentally-validated symmetry-based model along with normal mode analysis of a structure of *E. coli* NhaA suggest that a panel of four TM helices in NhaA may rotate within the plane of the membrane and around the transport domain in

order to open and close the inward and outward-facing pathways[23]. However, upon elucidation of the structure of NapA, a remote NhaA homolog, and subsequent structural comparison with NhaA, it has been argued that substrate-binding residues in NapA move 10 Å in the membrane, consistent with an elevator-type movement[14]. A caveat here is that NapA shares <15% identical residues with NhaA, making any conclusions drawn from the direct comparison of the two proteins somewhat tenuous. More recently, and contrary to the conclusions drawn from the NapA structure, structural analysis of two other CPA family members, PaNhaP and MjNhaP1, both solved in two conformations, suggest that only slight conformational changes are required for transport[29,30]. The structure of a bacterial concentrative nucleoside transporter, VcCNT, also reveals the hallmarks of an elevator-type transporter, although its structure has so far only been captured in an inward-facing state[31,32]. Interestingly, repeat-swap modeling predicts an elevator-type movement for this protein (Vergara-Jaque, Fenollar-Ferrer, Kaufmann and Forrest, under review) though this prediction has not yet been experimentally tested.

*Common features of elevator-type transporters*

Several shared structural features are immediately apparent upon looking at the structures of $Glt_{Ph}$, VcINDY and VcCNT. All three transporters have similar overall architecture, with a scaffold domain wrapped around a transport domain, and all are oligomers (VcINDY is a dimer, $Glt_{Ph}$ and VcCNT are trimers), possibly to aid in stabilization. In all three cases, the transport domain contains two re-entrant hairpin loops that dip into the membrane but do not cross it: the tips of these re-entrant loops coordinate substrates in all three transporters. Finally, all three folds contain a broken helix whose two segments are connected through an intramembrane loop (helices 5 and 10 in VcINDY, see Fig. 2a) that also contributes to the substrate-binding region.

Seemingly, a major mechanistic difference between $Glt_{Ph}$ and VcINDY is that in $Glt_{Ph}$ the re-entrant hairpin loops act as inner and outer gates that cover the substrate binding site and regulate substrate binding/release. In both the inward-facing structure and the outward-facing model of VcINDY, the substrate is almost completely solvent exposed (Fig. 2), obviating the need for such gate movement.

However, the electron density in the VcINDY crystal structure is ascribed to citrate, which is, in fact, a low affinity inhibitor[16]. Thus, our current analysis of the inhibitor-bound structure/model may miss some more subtle structural changes, for example, gate movement. Structural data for substrate-bound VcINDY will be required to uncover such details.

*How widespread is the elevator-type mechanism?*

Recent reports provide evidence that several transporter families have essentially the same fold as VcINDY. These transporters include the human $Na^+$/Pi transporter, NaPi[33]; and two recently structurally characterized representatives from the *p*-aminobenzoyl-glutamate transporter (AbgT) family, YdaH and MtrF[34,35]. The DASS family, to which VcINDY belongs, and the AbgT family, have both been assigned to the Ion Transporter (IT) superfamily, begging the tantalizing question; is the elevator-type movement a common mechanism for all IT superfamily members? Obviously, the mechanism underlying transport by the other IT superfamily members must be investigated, but the commonality of this architecture hints at widespread use of this mechanism.

Mammalian homologs of VcINDY are potential drug targets in the treatment of metabolic diseases, age-related diabetes and obesity[15,36]. VcINDY is ~30% identical and shares a number of functional characteristics, such as substrate specificity and coupling ion stoichiometry, with its mammalian homologs, in particular hNaDC3[16]. In addition, both VcINDY and hNaDC3 are allosterically inhibited by the anthranilic acid derivative, flufenamic acid, which is thought to interact at the interface between the scaffold and the transport domain[16,37,38]. These fundamental mechanistic similarities strongly suggest that the overall architecture and basic mechanism of transport are similar in all members of the DASS family. By extension, it would appear that the elevator-type motion is also an essential part of the transport cycle in the mammalian counterparts. Further work is required to explicitly demonstrate a shared structural mechanism for this family of transporters.

*What is the advantage of an elevator mechanism?*

Why would the elevator-type mechanism be favored over other transport mechanisms such as, say a "rocking bundle" mechanism? One apparently common characteristic of several potential elevator-type transporters is the tendency to couple substrate transport to multiple (≥3) coupling ions. At equilibrium, increasing the number of coupling ions (*n*) dramatically increases the capacity for substrate accumulation, with this increase changing as the *n*th power of the ion gradient. An elevator mechanism might be a useful way to insulate the transporter from back-leak of substrate or coupling ions, since it can never contain a continuous return path. Increasing the prevalence of well-studied elevator transporters will be necessary to evaluate this possibility.

## Methods

Model building

A VcINDY outward-facing model was obtained by applying the repeat-swapped homology modeling technique following a recently revised protocol (Vergara-Jaque, Fenollar-Ferrer, Kaufmann and Forrest, under review). The repeats in the VcINDY structure, PDB ID: 4F35[18], were defined as comprising residues 42-242 for repeat unit 1 (RU1) and 253-462 for repeat unit 2 (RU2). The analysis of the symmetry axis of the repeats was performed using SymD[39]. TM-align was used to structurally superimpose these repeats[40], and to build an initial sequence alignment of the template and the model sequences. This initial alignment was refined by removing gaps within secondary structural elements (obtained from DSSP[41,42]) and by using conservation scores (obtained from the ConSurf server with default settings[43]) to position conserved residues so that they were preferentially oriented toward the inside of the protein For each refinement step, 200 iterations of restraint optimization were performed using Modeller v9.13[44]. Each set of models was evaluated using MolPDF and ProQM[45] scores as well as Procheck analysis[45,46].

The refined, final alignment was then used to generate a set of 2000 repeat-swapped 3D models of which the best model was selected as that which best met the following criteria: the lowest MolPDF score, the highest global ProQM scores, and the most residues in favored regions of the Ramachandran

plot. This model was then used to identify the scaffold and transport domains, which were assigned as residues 19-126 plus 253-356, and 127-242 plus 357-462, respectively. Final refinement of the model involved adding distance restraints between Cα atoms taken from the known structure in addition to those necessary to position the ions and bound ligand in the binding site. Distance restraints between Cα atoms were assigned according to the input crystal structure for all pairs of Cα atoms <60 Å apart within either the transport or scaffold domains in the template structure, PDB ID: 4F35[18]. We note that these intradomain restraints did not alter the extent of the conformational movement, but maintained the internal arrangement of the two domains (Supplementary Figs. 2b and 7). Distance restraints were also applied in the substrate binding sites: between the $Na^+$ ion and the O atoms in the backbone of S146, S150 and N199, the hydroxyl group of S146 and the amide group of N151; and between any non-hydrogen atoms of the citrate and the protein within 3.5 Å in the template structure. All applied distance restraints were represented as Gaussians with a standard deviation of 0.1 Å. Using these restraints, a new set of 2000 models was generated using Modeller, and again the final model was chosen using the criteria mentioned above.

The orientation of the VcINDY X-ray structure in the membrane was determined with the OPM server[47], while the orientation of the model was defined after superposition of the scaffold domain onto the crystal structure. For the analysis of the transport-scaffold interface, we selected all residues with any atom within 5 Å of the other domain in either inward- or outward-facing conformation. In the case of $Glt_{Ph}$ PDB entries 3KBC (inward-facing) and 1XFH (outward-facing) were used. All molecular figures and movies were generated using PyMOL v1.6 (Schrödinger, Ltd) unless stated otherwise. The final model is provided as Supplementary Data.

Molecular biology

All mutants were made using the Quikchange II site directed mutagenesis kit (Agilent Technologies) and were fully sequenced to ensure sequence fidelity. All cysteine mutants were

generated in cysteine-free background where all three native cysteines in VcINDY were substituted for serine.

Protein expression and purification

VcINDY and its variants were expressed and purified as detailed previously[18]. VcINDY was expressed in *Escherichia coli* BL21-AI cells (Life Technologies) from a modified pET vector in frame with a N-terminal decahistidine tag[48]. Cells were grown in LB supplemented with 30 ug/ml kanamycin at 37°C until they reached an $A_{600}$ of 0.8, at which point they were rapidly cooled to 19°C in an ice bath. Expression was induced by addition of IPTG and L-arabinose to final concentrations of 10 μM and 6.6 mM, respectively. Cells were incubated overnight at 19°C. Cells were harvested and resuspended in Lysis Buffer (50 mM Tris, pH 8, 400 mM NaCl and 20% glycerol), and lysed using a homogenizer (Emulsiflex-C3, Avestin). The membrane fraction was isolated by ultracentrifugation, resuspended in Purification Buffer (50 mM Tris, pH 8, 200 mM NaCl and 10% glycerol), and solubilized by addition of *n*-dodecyl-β-D-maltoside (DDM, Anatrace) to a final concentration of 20 mM. Residual insoluble material was removed by ultracentrifugation and the soluble fraction was incubated with Talon metal affinity resin (Takara Bio Inc.) overnight at 4°C. Resin was washed by consecutive additions of 20 column volumes-worth of 10 mM and 20 mM imidazole-containing Purification Buffer supplemented with 2 mM DDM. Bound protein was eluted whilst simultaneously cleaving the affinity tag by incubating the resin with Purification Buffer supplemented with 2 mM DDM and 10 μg/ml trypsin at 4°C for 1 hour. The flowthrough from the column was collected, concentrated and further purified using a Superdex 200 size exclusion chromatography (SEC) column (GE Healthcare) equilibrated with SEC buffer (25 mM Tris pH, 100 mM NaCl, 5% glycerol and 3 % *n*-decyl-β-D-maltoside (DM)). For the dimer interface mutants, protein was eluted from the Talon resin by addition of Purification Buffer supplemented with 300 mM imidazole. The affinity tag was maintained for identification of the protein using Western blotting. The dimer interface mutants were then desalted into SEC buffer using Zeba Spin desalting columns (Life Technologies). Purified protein was concentrated, snap frozen and stored at -80°C. All proteins were purified using buffers containing

either 0.5 mM tris(2-carboxyethyl)phosphine (TCEP) or 1 mM dithiothreitol (DTT) to keep the cysteines reduced.

Reconstitution

The functional reconstitution of protein into liposomes was performed as detailed previously[49]. 25-100 μg of purified protein was diluted to 2 ml in SEC buffer (with 1 mM DTT, if required) and mixed with 400 μl 20 mg/ml lipids, which consisted of a 3:1 mixture of *E. coli* polar lipids and POPC (Avanti Polar Lipids, Inc). The protein/lipid mixture was incubated on ice for 10 min and then rapidly diluted into 65 ml Inside Solution containing 20 mM Tris/HEPES, pH 7.5, 1 mM NaCl, 199 mM KCl and 0.5 mM TCEP/1 mM DTT, where required. Proteoliposomes were collected by ultracentrifugation and resuspended in Inside Solution to a concentration of 8 mg/ml lipid. Proteoliposomes were freeze-thawed 3 times and stored at -80°C or used immediately. After this point, the internal solution was modified by collecting the proteoliposomes by centrifugation, resuspending them in the desired solution, freeze-thawing 3 times and extruding.

*In vitro* transport assays

Proteoliposomes were prepared for transport assays by extruding them through a 400 nm filter 11 times and concentrating them to 80 mg/ml lipid using ultracentrifugation. The transport assays were started by adding the proteoliposomes to Reaction Buffer (20 mM Tris/HEPES, pH 7.5, 100 mM NaCl, 100 mM KCl, 1 μM valinomycin, 1 μM [$^3$H]-succinic acid (American Radiolabeled Chemicals). At the indicated times, samples were taken and the reaction was terminated by adding the sample to ice cold Quench buffer (20 mM Tris/HEPES, pH 7.5, 200 mM ChCl) and rapidly filtering the sample through a 200 nm nitrocellulose filter (Millipore). The filter was washed with 3 ml Quench buffer, the filters were dissolved in FilterCount liquid scintillation cocktail (PerkinElmer) and the [$^3$H]-succinic acid internalized by the proteoliposomes was counted using a Trilux beta counter (PerkinElmer).

Protein crosslinking and PEGylation assay

To induce disulfide bond formation, the proteins were exchanged into Conjugation Buffer (50 mM Tris, pH 7, 100 mM NaCl, 5 % glycerol, and 3% (w/v) DM) to remove the reducing agent and then

incubated with 5-fold molar excess of $HgCl_2$ or freshly prepared solution of copper phenanthroline (CuPhen). A 2:1 ratio of CuPhen was prepared by mixing solutions of 500 mM 1,10-phenanthroline and 250 mM $CuSO_4$. The final CuPhen concentration ranged from 10 to 500 μM depending on the particular cysteine mutant. Regardless of which crosslinking reagent was being used, the crosslinking reaction was incubated at room temperature for 45 min. Control samples were treated identically except were incubated in the presence of 0.5 mM TCEP or 1 mM DTT.

Protein Digestion and Mass Spectrometry

Protein samples, at 10 μM, in 50 mM Tris pH 7, 150 mM NaCl, 5% glycerol, 0.1% DM were either reduced with 1 mM DTT ('R') or treated with 100 μM or 500 μM CuPhen to induce disulfide formation ('X') followed by desalting to remove the reagent. ~5 μg of protein was alkylated by incubation with 10 mM N-ethylmaleimide (NEM, Sigma) for 20 min at room temperature. A120C/V165C was digested with 500 ng trypsin for 8 hr at 37°C and further digested with 300 ng chymotrypsin (Roche, Indianapolis, IN) for 8 hr at 25°C ; T154C/V272C was digested with 600 ng chymotrypsin at 25°C overnight. The digests were cleaned with an HLB μElution plate (Waters, Milford, MA). The LC/MS/MS experiments were performed on an Orbitrap Elite mass spectrometer (Thermo Scientific) connected to a 3000 RSLC nano HPLC system with an RS auto-sampler (Thermo-Dionex) via an Easy-Spray ion source (Thermo Scientific). Approximately 1 μg of digested protein was injected onto an ES802 Easy-Spray column (25cm x 75μm ID, PepMap RSLC C18 2μm; Thermo Scientific) and then separated at a flow rate of 300 nl/min with a 38 min linear gradient of 2–30% mobile phase B (mobile phase A: 2% acetonitrile, 0.1% formic acid; mobile phase B: 98% acetonitrile, 0.1% formic acid).

The Orbitrap Elite was operated in a decision tree mode. The precursor ion scan was performed in the Orbitrap with a resolution of 60K at m/z 400. The m/z range for survey scans was 300–1600. The fragment ion scan was performed in the linear ion trap. The minimum signal threshold for MS/MS scan was set to $3 \times 10^4$, and up to 10 MS/MS scans were performed after each MS scan. A 9 sec dynamic exclusion window was selected with early expiration enabled.

Peptide Identification

Mascot Distiller (version 2.5.1.0) was used to convert the Xcalibur Raw data to peak list file in mgf format. Mascot Daemon 2.4.0 was used to submit the MGF files to Mascot Server 2.4 for the database search. Data were searched against a house-built database that contains the sequences of NCBI human database and the sequences of 120/165-R, 120/165-X, 154/272-R and 154/272-X. The following parameters were included in the search: Peptide tolerance, ± 10 ppm; MS/MS tolerance, 0.2 Da; Instrument type, CID+ETD; Enzyme, None; Missed cleavage, 0; Variable modification, Oxidation (M) and NEM (C). Once a peptide (Px) containing a Cys residue was detected, a 2$^{nd}$ database search was performed assuming Px-2H (the mass of Px minus 2 hydrogen atoms) as a potential modification. Once a plausible cross-linked candidate was found in the 2$^{nd}$ search, the MS/MS spectrum of that candidate was manually checked. A potentially cross-linked candidate was considered real if the following conditions were satisfied: 1) Major peaks of the MS/MS spectrum of the cross-linked candidate could be assigned manually; 2) The candidate was only detected in the X samples, not in the corresponding R samples.

**Reference List**


1. Jardetzky, O. Simple allosteric model for membrane pumps. *Nature* **211**, 969-70 (1966).
2. Mitchell, P. A general theory of membrane transport from studies of bacteria. *Nature* **180**, 134-6 (1957).
3. Krishnamurthy, H., Piscitelli, C.L. & Gouaux, E. Unlocking the molecular secrets of sodium-coupled transporters. *Nature* **459**, 347-55 (2009).
4. Yamashita, A., Singh, S.K., Kawate, T., Jin, Y. & Gouaux, E. Crystal structure of a bacterial homologue of Na+/Cl--dependent neurotransmitter transporters. *Nature* **437**, 215-23 (2005).
5. Reddy, V.S., Shlykov, M.A., Castillo, R., Sun, E.I. & Saier, M.H., Jr. The major facilitator superfamily (MFS) revisited. *FEBS J* **279**, 2022-35 (2012).
6. Vastermark, A. & Saier, M.H., Jr. Evolutionary relationship between 5+5 and 7+7 inverted repeat folds within the amino acid-polyamine-organocation superfamily. *Proteins* **82**, 336-46 (2014).
7. Fowler, P.W. et al. Gating topology of the proton-coupled oligopeptide symporters. *Structure* **23**, 290-301 (2015).
8. Kazmier, K., Sharma, S., Islam, S.M., Roux, B. & McHaourab, H.S. Conformational cycle and ion-coupling mechanism of the Na+/hydantoin transporter Mhp1. *Proc Natl Acad Sci U S A* **111**, 14752-7 (2014).
9. Kazmier, K. et al. Conformational dynamics of ligand-dependent alternating access in LeuT. *Nat Struct Mol Biol* **21**, 472-9 (2014).
10. Krishnamurthy, H. & Gouaux, E. X-ray structures of LeuT in substrate-free outward-open and apo inward-open states. *Nature* **481**, 469-74 (2012).
11. Shimamura, T. et al. Molecular basis of alternating access membrane transport by the sodium-hydantoin transporter Mhp1. *Science* **328**, 470-3 (2010).
12. Crisman, T.J., Qu, S., Kanner, B.I. & Forrest, L.R. Inward-facing conformation of glutamate transporters as revealed by their inverted-topology structural repeats. *Proc Natl Acad Sci U S A* **106**, 20752-7 (2009).
13. Reyes, N., Ginter, C. & Boudker, O. Transport mechanism of a bacterial homologue of glutamate transporters. *Nature* **462**, 880-5 (2009).
14. Lee, C. et al. A two-domain elevator mechanism for sodium/proton antiport. *Nature* **501**, 573-7 (2013).
15. Bergeron, M.J., Clemencon, B., Hediger, M.A. & Markovich, D. SLC13 family of Na(+)-coupled di- and tri-carboxylate/sulfate transporters. *Mol Aspects Med* **34**, 299-312 (2013).
16. Mulligan, C., Fitzgerald, G.A., Wang, D.N. & Mindell, J.A. Functional characterization of a Na+-dependent dicarboxylate transporter from Vibrio cholerae. *J Gen Physiol* **143**, 745-59 (2014).
17. Saier, M.H., Jr., Tran, C.V. & Barabote, R.D. TCDB: the Transporter Classification Database for membrane transport protein analyses and information. *Nucleic Acids Res* **34**, D181-6 (2006).
18. Mancusso, R., Gregorio, G.G., Liu, Q. & Wang, D.N. Structure and mechanism of a bacterial sodium-dependent dicarboxylate transporter. *Nature* **491**, 622-6 (2012).
19. Chen, J.S. et al. Phylogenetic characterization of transport protein superfamilies: superiority of SuperfamilyTree programs over those based on multiple alignments. *J Mol Microbiol Biotechnol* **21**, 83-96 (2011).
20. Prakash, S., Cooper, G., Singhi, S. & Saier, M.H., Jr. The ion transporter superfamily. *Biochim Biophys Acta* **1618**, 79-92 (2003).
21. Forrest, L.R. et al. Mechanism for alternating access in neurotransmitter transporters. *Proc Natl Acad Sci U S A* **105**, 10338-43 (2008).
22. Radestock, S. & Forrest, L.R. The alternating-access mechanism of MFS transporters arises from inverted-topology repeats. *J Mol Biol* **407**, 698-715 (2011).
23. Schushan, M. et al. A model-structure of a periplasm-facing state of the NhaA antiporter suggests the molecular underpinnings of pH-induced conformational changes. *J Biol Chem* **287**, 18249-61 (2012).

24. Basilio, D., Noack, K., Picollo, A. & Accardi, A. Conformational changes required for H(+)/Cl(-) exchange mediated by a CLC transporter. *Nat Struct Mol Biol* **21**, 456-63 (2014).
25. Groeneveld, M. & Slotboom, D.J. Rigidity of the subunit interfaces of the trimeric glutamate transporter GltT during translocation. *J Mol Biol* **372**, 565-70 (2007).
26. Forrest, L.R. Structural Symmetry in Membrane Proteins. *Annu Rev Biophys* **44**, 311-37 (2015).
27. Forrest, L.R., Tang, C.L. & Honig, B. On the accuracy of homology modeling and sequence alignment methods applied to membrane proteins. *Biophys J* **91**, 508-17 (2006).
28. Yernool, D., Boudker, O., Jin, Y. & Gouaux, E. Structure of a glutamate transporter homologue from Pyrococcus horikoshii. *Nature* **431**, 811-8 (2004).
29. Paulino, C., Wohlert, D., Kapotova, E., Yildiz, O. & Kuhlbrandt, W. Structure and transport mechanism of the sodium/proton antiporter MjNhaP1. *Elife* **3**, e03583 (2014).
30. Wohlert, D., Kuhlbrandt, W. & Yildiz, O. Structure and substrate ion binding in the sodium/proton antiporter PaNhaP. *Elife* **3**, e03579 (2014).
31. Johnson, Z.L., Cheong, C.G. & Lee, S.Y. Crystal structure of a concentrative nucleoside transporter from Vibrio cholerae at 2.4 A. *Nature* **483**, 489-93 (2012).
32. Johnson, Z.L. et al. Structural basis of nucleoside and nucleoside drug selectivity by concentrative nucleoside transporters. *Elife* **3**, e03604 (2014).
33. Fenollar-Ferrer, C. et al. Structural fold and binding sites of the human Na(+)-phosphate cotransporter NaPi-II. *Biophys J* **106**, 1268-79 (2014).
34. Bolla, J.R. et al. Crystal structure of the Alcanivorax borkumensis YdaH transporter reveals an unusual topology. *Nat Commun* **6**, 6874 (2015).
35. Su, C.C. et al. Structure and function of Neisseria gonorrhoeae MtrF illuminates a class of antimetabolite efflux pumps. *Cell Rep* **11**, 61-70 (2015).
36. Colas, C., Pajor, A.M. & Schlessinger, A. Structure based identification of inhibitors for the SLC13 family of Na+/dicarboxylate cotransporters. *Biochemistry* (2015).
37. Burckhardt, B.C., Lorenz, J., Burckhardt, G. & Steffgen, J. Interactions of benzylpenicillin and non-steroidal anti-inflammatory drugs with the sodium-dependent dicarboxylate transporter NaDC-3. *Cell Physiol Biochem* **14**, 415-24 (2004).
38. Pajor, A.M. & Sun, N.N. Nonsteroidal anti-inflammatory drugs and other anthranilic acids inhibit the Na(+)/dicarboxylate symporter from Staphylococcus aureus. *Biochemistry* **52**, 2924-32 (2013).
39. Tai, C.H., Paul, R., Dukka, K.C., Shilling, J.D. & Lee, B. SymD webserver: a platform for detecting internally symmetric protein structures. *Nucleic Acids Res* **42**, W296-300 (2014).
40. Zhang, Y. & Skolnick, J. TM-align: a protein structure alignment algorithm based on the TM-score. *Nucleic Acids Res* **33**, 2302-9 (2005).
41. Kabsch, W. & Sander, C. Dictionary of protein secondary structure: pattern recognition of hydrogen-bonded and geometrical features. *Biopolymers* **22**, 2577-2637 (1983).
42. Edgar, R.C. Quality measures for protein alignment benchmarks. *Nucleic Acids Research* **38**, 2145-2153 (2010).
43. Ashkenazy, H., Erez, E., Martz, E., Pupko, T. & Ben-Tal, N. ConSurf 2010: calculating evolutionary conservation in sequence and structure of proteins and nucleic acids. *Nucleic Acids Res* **38**, W529-33 (2010).
44. Šali, A. & Blundell, T.L. Comparative protein modelling by satisfaction of spatial restraints. *J. Mol. Biol.* **234**, 779-815 (1993).
45. Ray, A., Lindahl, E. & Wallner, B. Model quality assessment for membrane proteins. *Bioinformatics* **26**, 3067-74 (2010).
46. Laskowski, R.A., Macarthur, M.W., Moss, D.S. & Thornton, J.M. PROCHECK - A program to check the stereochemical quality of protein structures. *J. Appl. Crystall.* **26**, 283-291 (1993).
47. Lomize, M.A., Lomize, A.L., Pogozheva, I.D. & Mosberg, H.I. OPM: orientations of proteins in membranes database. *Bioinformatics* **22**, 623-5 (2006).

48. Love, J. et al. The New York Consortium on Membrane Protein Structure (NYCOMPS): a high-throughput platform for structural genomics of integral membrane proteins. *J Struct Funct Genomics* **11**, 191-9 (2010).
49. Mulligan, C. et al. The substrate-binding protein imposes directionality on an electrochemical sodium gradient-driven TRAP transporter. *Proc Natl Acad Sci U S A* **106**, 1778-83 (2009).
50. Krebs, W.G. & Gerstein, M. The morph server: a standardized system for analyzing and visualizing macromolecular motions in a database framework. *Nucleic Acids Res* **28**, 1665-75 (2000).
51. Dahl, A.C., Chavent, M. & Sansom, M.S. Bendix: intuitive helix geometry analysis and abstraction. *Bioinformatics* **28**, 2193-4 (2012).
52. Humphrey, W., Dalke, A. & Schulten, K. VMD: visual molecular dynamics. *J Mol Graph* **14**, 33-8, 27-8 (1996).

**Figure 1**

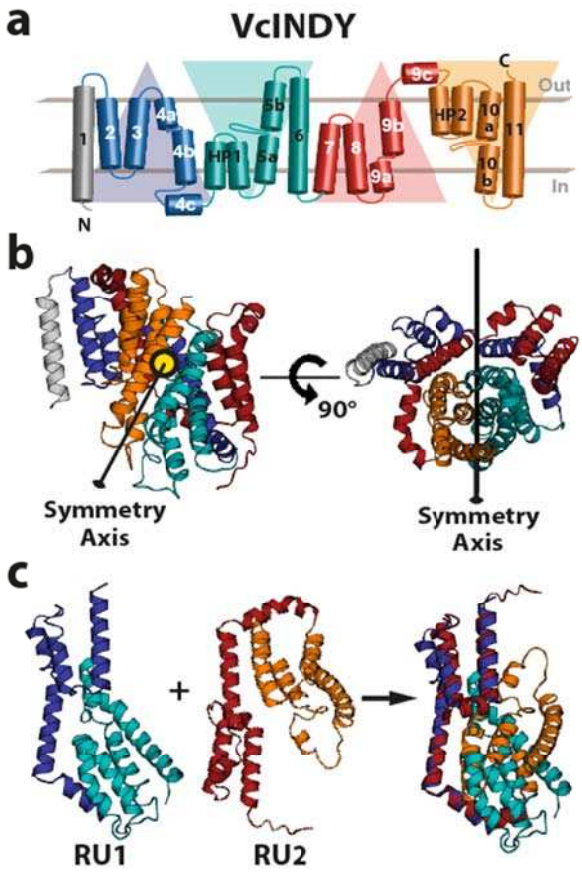


**Figure 1. Repeat-swap modeling of VcINDY. (a)** Schematic representation of the topology of VcINDY colored according to the structural repeats. The blue and cyan helices comprise repeat unit 1 (RU1), while repeat unit 2 (RU2) is composed of the red and orange helices. **(b)** RU1 is related to RU2 by two-fold pseudo-symmetry, with the symmetry axis parallel to the membrane. The black arrow represents the symmetry axis within the structure of the VcINDY protomer, viewed from within the plane of the membrane (*left*) and from the extracellular side of the protein (*right*). **(c)** A structural alignment, built with TM-Align, of the repeats is shown in cartoon representation with the helices colored according to the topology in **(a)**. The initial sequence alignment used to build a swapped-repeat model was generated based on this structural alignment.

**Figure 2**

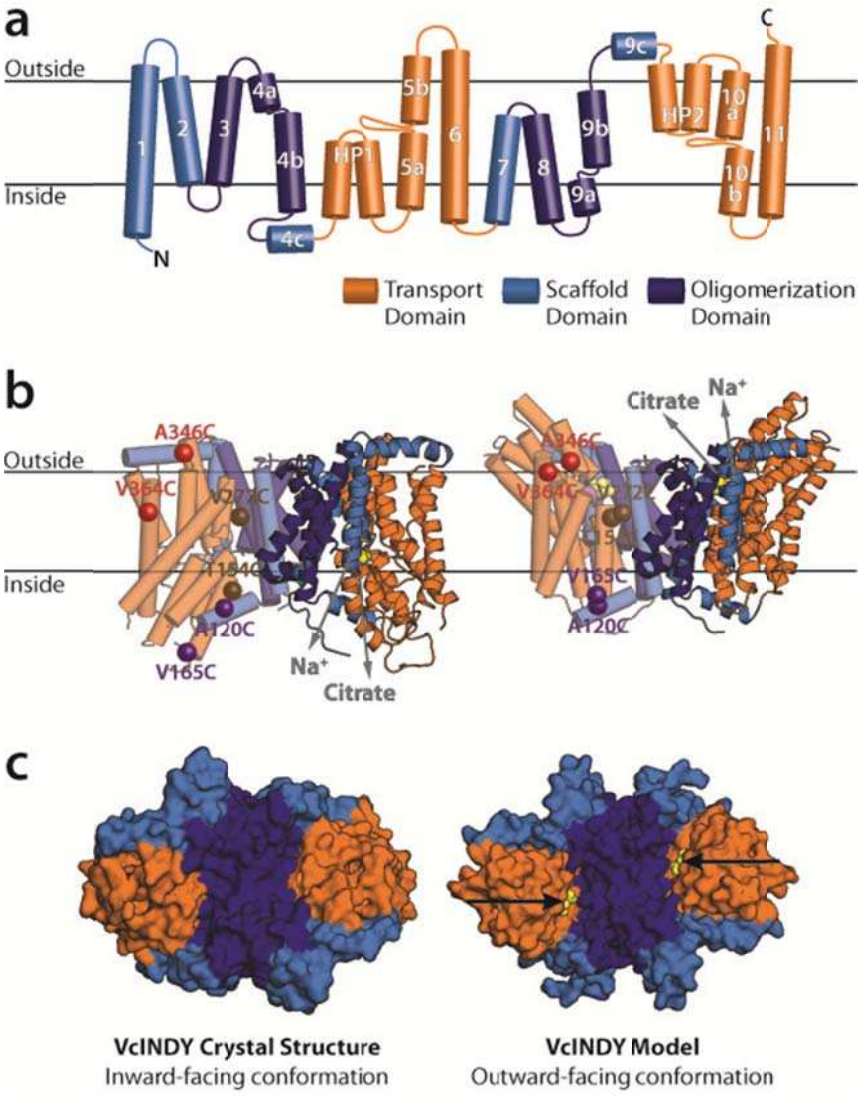


**Figure 2. Identification of the scaffold, oligomerization and transport domains of the VcINDY transporter**. **(a)** Topology diagram of a VcINDY protomer colored according to the helices forming the scaffold (*light blue*), oligomerization (*dark blue*) and transport (*orange*) domains. **(b)** Cartoon representation of the dimeric VcINDY X-ray crystal structure in an inward-facing conformation (*left*) and the model in an outward-facing conformation (*right*) viewed from the membrane plane. Substrates (citrate and $Na^+$) are shown as spheres, with their pathways indicated by gray arrows. C$\alpha$-atoms of the residues studied by crosslinking are shown as spheres colored in pairs (*left-hand side protomers*). **(c)** Surface representation of the VcINDY X-ray crystal structure (*left*) and model (*right*) viewed from the

extracellular side. The substrate (yellow spheres, indicated by arrows) is visible from the extracellular side in the model (*right*), but not in the inward-facing crystal structure (*left*).

**Figure 3**

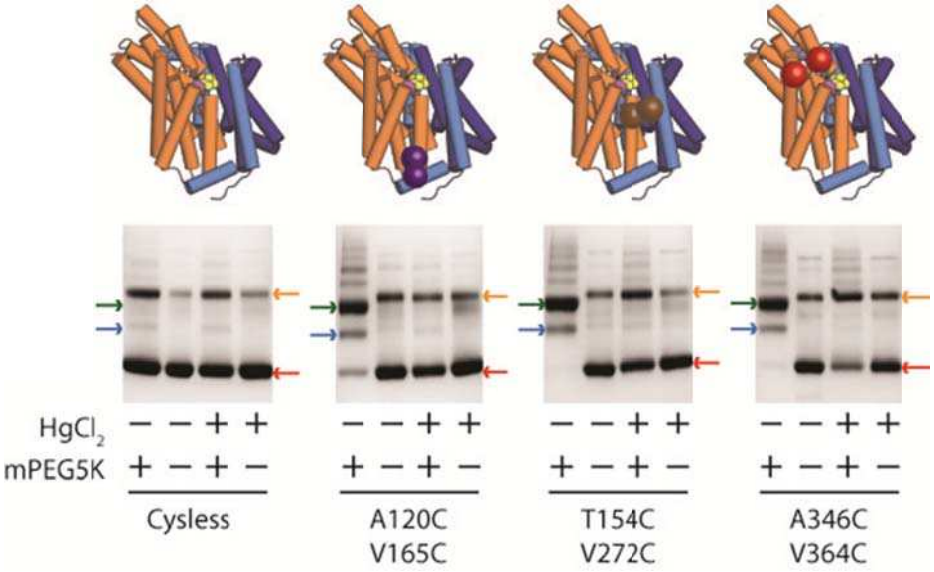


**Figure 3. Chemical crosslinking protects outward-stabilizing cysteine pairs from mPEG5K labeling.** SDS-PAGE band-shift assay showing the number of free cysteines present in Cysless and the three double cysteine mutants; A120C/V165C, T154C/V272C, and A346C/V364C, with (+) and without (-) prior treatment with $HgCl_2$. Relative positions of the cysteine pairs are shown in the cartoon representation of a VcINDY protomer (*top*). The following protein species seen in the gels are indicated by colored arrows; unmodified VcINDY (*red arrow*), dimeric VcINDY (*orange arrow*), singly PEGylated VcINDY (*blue arrow*), and doubly PEGylated VcINDY (*green arrow*).

**Figure 4**

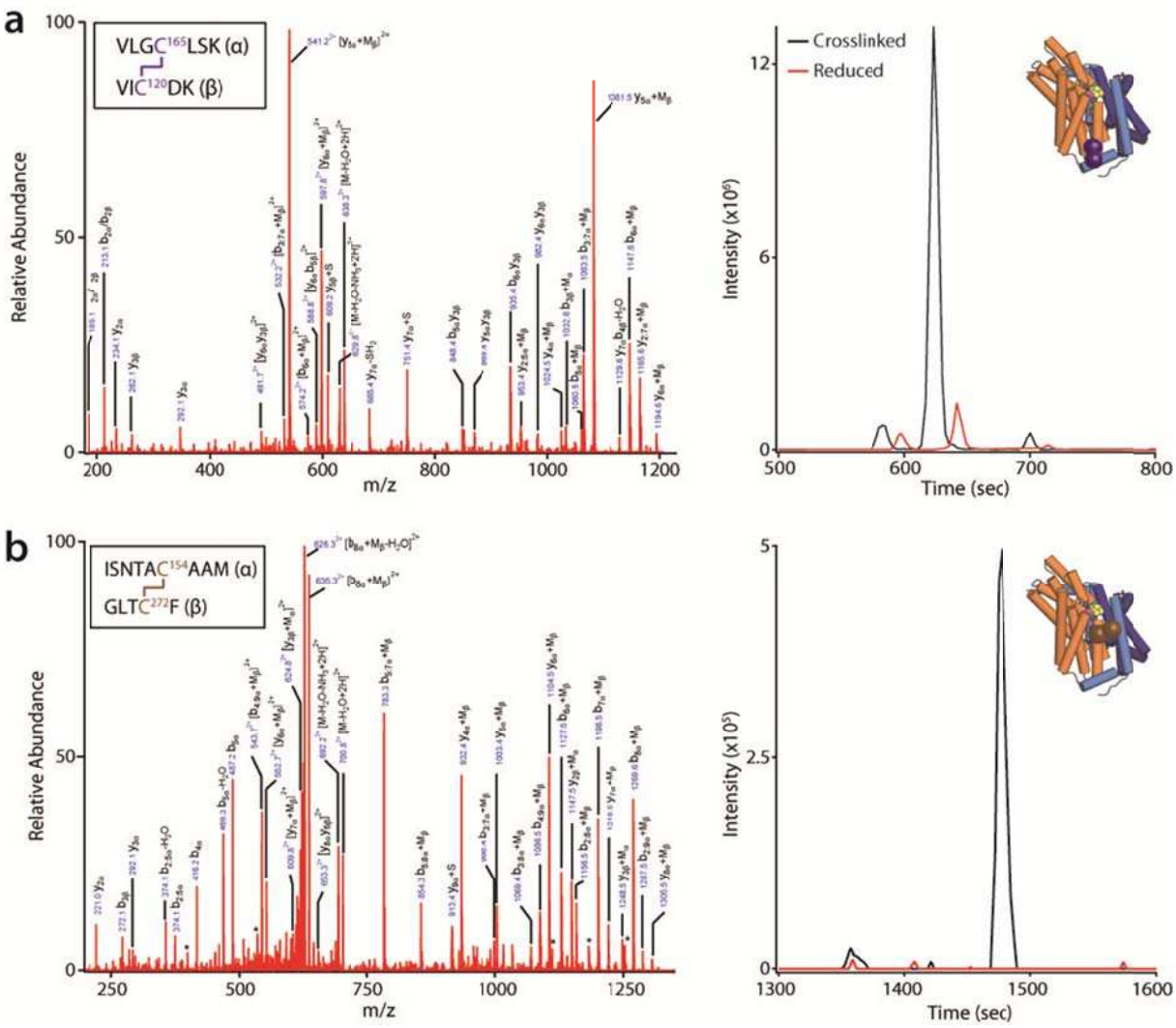


**Figure 4. Mass spectrometric identification of crosslinked peptides.** Representative LC-MS/MS data for **(a)** A120C/V165C and **(b)** T154C/V272C. Collision-induced dissociation (CID) spectrum of the disulfide linked peptide (shown inset) from the proteolytic digests (*left*), and the associated extracted ion chromatogram (XIC) for protein treated with crosslinking reagent (*black lines*) or maintained in reducing conditions (*red line*).

**Figure 5**

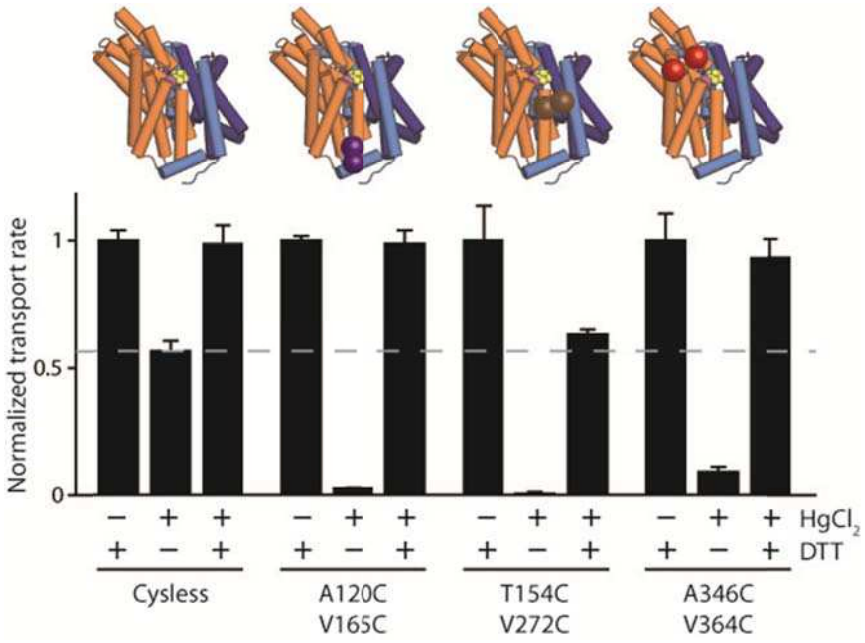


**Figure 5. Stabilizing VcINDY in the outward-facing state abolishes transport activity.** Normalized initial rates of [$^3$H]-succinate transport in the presence of proteoliposomes containing Cysless and the three double cysteine mutants compatible with the outward-facing state after treatment with (+) and without (-) $HgCl_2$ and DTT. Relative positions of cysteine pairs are shown as in Fig. 3. Results from triplicate datasets are shown and error bars represent S.E.M.

**Figure 6**

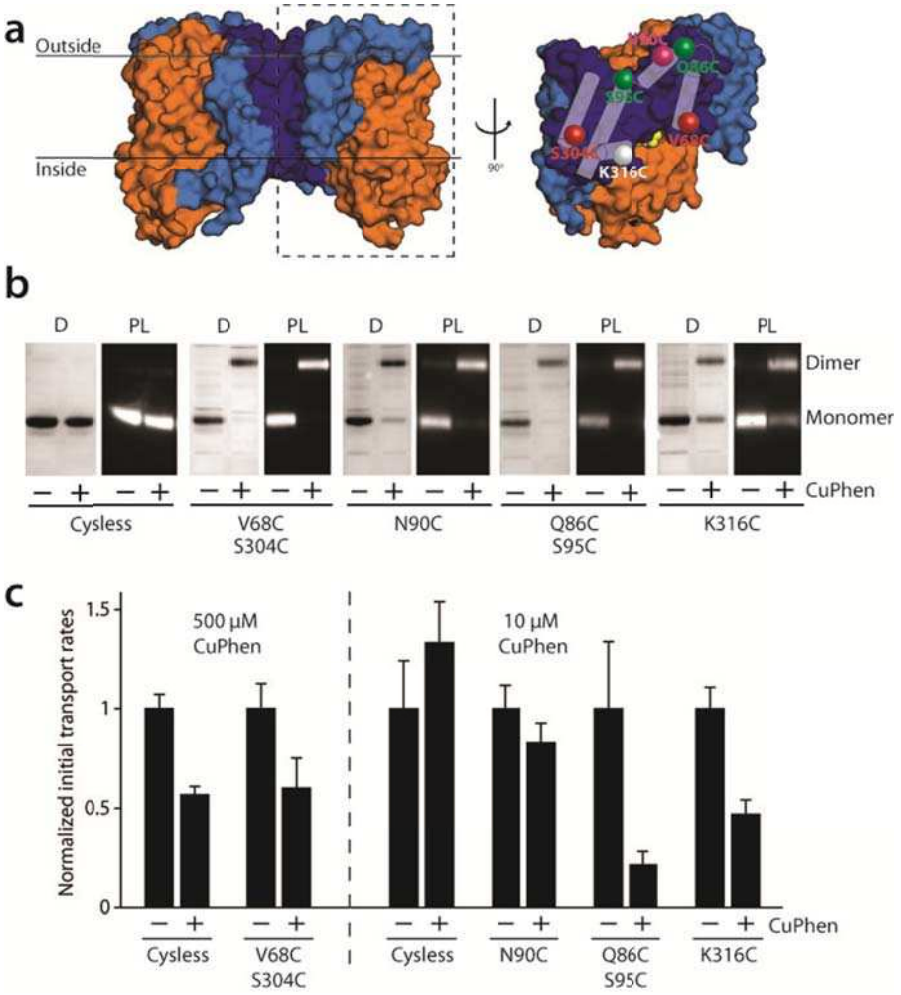


**Figure 6. Constraining the dimer interface has minimal effects on transport activity. (a)** Surface representation of a VcINDY dimer viewed from the plane of the membrane (*left*) and a VcINDY protomer viewed from the dimer interface (*right*), if the VcINDY dimer is opened like a book. White cylinders represent the interfacialα-helices that make the intra-protomer contacts across the dimer interface. The colored spheres represent the positions of cysteine residues introduced to staple the VcINDY protomers together. **(b)** Coomassie-stained SDS-PAGE gels of purified cysteine mutants in detergent solution ('D') and His-tag Western blot analysis of VcINDY-containing proteoliposomes ('PL') with (+) and without (-) treatment with CuPhen. The positions of monomeric and dimeric VcINDY are indicated. **(c)** Normalized initial transport rates of Cysless and indicated cysteine mutants with (+) and without (-) treatment with CuPhen. Results are from at least triplicate datasets and error bars represent S.E.M.

**Figure 7**

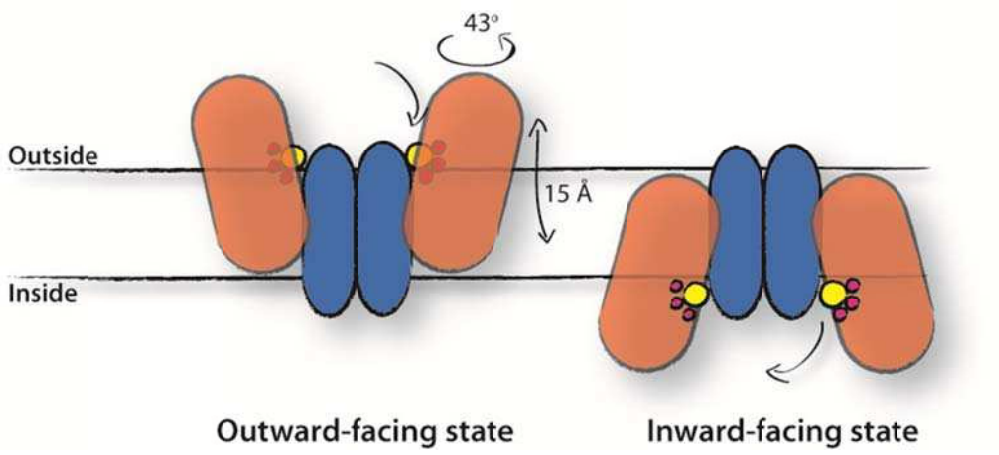


**Figure 7. Proposed elevator-type transport mechanism of VcINDY.** Cartoon representation of the transport mechanism inferred from the inward-facing crystal structure and outward-facing model of VcINDY. Blue shapes represent the scaffold/oligomerization domains and the orange shape is the transport domain. Substrates are represented by yellow spheres (citrate) and pink spheres ($Na^+$ ions). In our scheme, the substrates bind the outward-facing state of VcINDY (*left*, model) at which point the transport domain undergoes a ~15 Å translocation and 43° rotation into the inward-facing state (*right*, crystal structure), where substrate can be released into the cytoplasm. Empty transporter must then recycle back to the outward-facing state to restart the cycle.

**Supplementary Movie 1: Predicted transport-associated conformational change in VcINDY.** The conformational change predicted for VcINDY is modeled by morphing the VcINDY inward-facing X-ray structure (PDB ID: 4F35) (*start*) with the repeat-swapped model of the outward-facing conformation (*end point*). The interpolation between structure and model was done using the Morph2[50]. VcINDY is represented as cartoon helices and the coloring scheme reflects the division between scaffold (*blues*), oligomerization domain (*dark blue*) and transport domain (*orange*), as shown in Figure 1. The sodium ion and the citrate are shown as purple and yellow spheres, respectively. The protein is viewed from the plane of the membrane, first, from the perspective of the other protomer, and secondly, along the dimer axis.

**Supplementary Movie 2: Cross-linking during the transport-associated conformational change in VcINDY.** See legend to Supplementary Movie 1 for more detail. Here, the Cα atom of each of the residue pairs that crosslink in the outward-facing conformation is also shown as spheres, color-coded by crosslinking pair as follows: Ala120 and Val165 in magenta, Thr154 and Val272 in green and Ala346 and Val364 in red.

**Supplementary Figure 1**

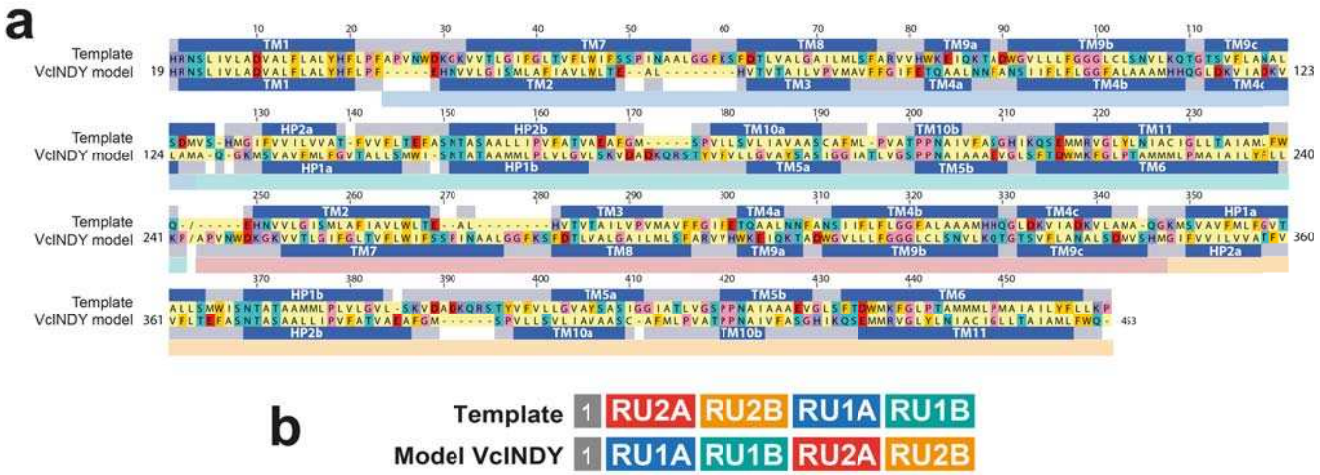


**Supplementary Figure 1. Sequence alignment for modeling. (a)** Refined sequence alignment between the template (i.e., reordered X-ray crystal structure), and the normal sequence of VcINDY, which corresponds to the repeat-swapped model. The percentage of identical residues is ~24% for the full-length alignment, including peripheral elements; within the repeats, ~20% of the residues are identical. The sequence range of each repeat is indicated by rectangles under the target sequences, colored as in Fig. 1a. The secondary structure (helix) assignment obtained with DSSP for the X-ray structure is indicated by dark blue rectangles. Amino acids are colored as followed: red for acidic (asp and glu), dark blue for basic (his, lys and arg), cyan for polar (ser, thr, asn, gln), yellow for aromatic (tyr, trp and phe), pink for helix-breaking (pro and gly), and pale yellow for cysteine and aliphatic (ala, val, ile, leu and met). **(b)** Schematic indicating which structural repeat segments (colored as in (a)) are modeled on which segments of the crystal structure template. The peripheral helices (TM 1) in the model and template are shown in gray.

**Supplementary Figure 2**

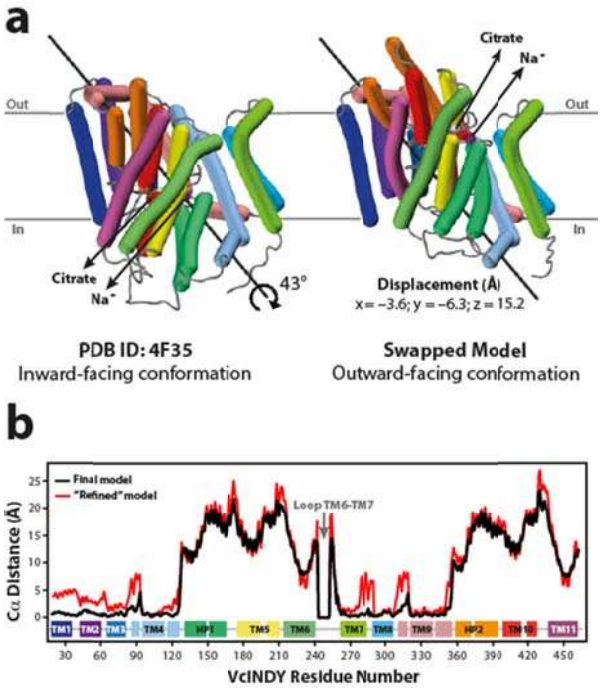


**Supplementary Figure 2. Crystal structure of VcINDY compared with the repeat-swapped model. (a)** The X-ray crystal structure of a VcINDY protomer in an inward-facing conformation (*left*) is compared with the repeat-swapped model in an outward-facing conformation (*right*). Structures are viewed along the plane of the membrane, with the extracellular side at the top. The Bendix plugin[51] to the program VMD[52] was used to represent the helices. To quantify the conformational change of the protein, the rotation axis, rotation angle and the displacement of the helices were evaluated. The black line indicates the rotation axis, which lies approximately perpendicular to the symmetry axis. The displacement values suggest an elevator-like movement of the transport domain containing the substrates (*spheres*) across the membrane, and this displacement is associated with a rotation of 43°. (**b**) Displacement per residue was determined as the distance between Cα atoms in the crystal structure and the model (*black line*) after aligning the structures using the scaffold domain. Note that the model built prior to adding intradomain restraints, but using the same refined alignment ("Refined model", *red line*) implies a similar conformational change in the transport domain relative to the scaffold as the model built using intradomain restraints ("Final model", *black line*). By this analysis, the transport domain can be considered to comprise helices HP1-TM5-TM6 and HP2-TM10-TM11.

**Supplementary Figure 3**

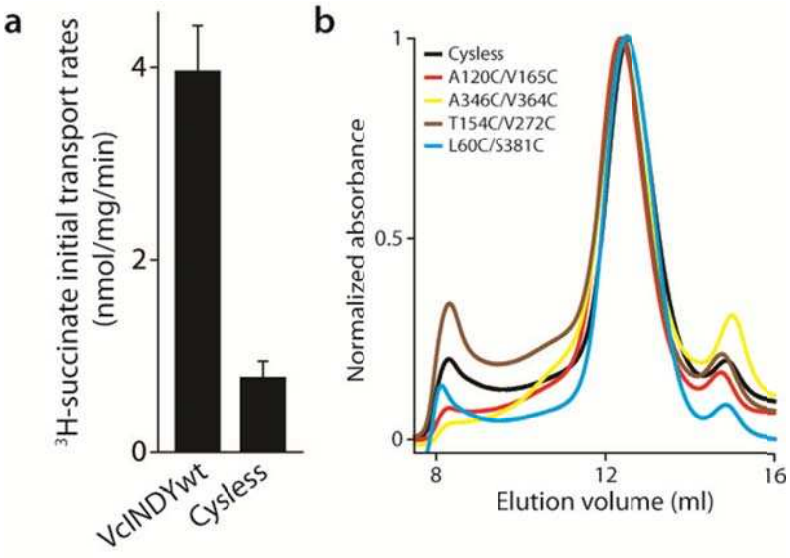


**Supplementary Figure 3. Activity and stability of cysteine mutants. (a)** Initial rates of $^3$H-succinate transport by wild type VcINDY (VcINDYwt) and cysteine-free VcINDY (Cysless) after reconstitution into liposomes. Triplicate datasets were used and error bars represent S.E.M. **(b)** Size exclusion chromatography (SEC) traces showing the normalized absorbance at $A_{280}$ for Cysless the 4 double cysteine mutants; A120C/V165C (*red*), A346C/V364C (*yellow*), T154C/V272C (*brown*), and L60C/S381C (*light blue*). $V_0$ is ~8 ml and VcINDY elution peak is centered on 12.5 ml on the S200 SEC column.

**Supplementary Figure 4**

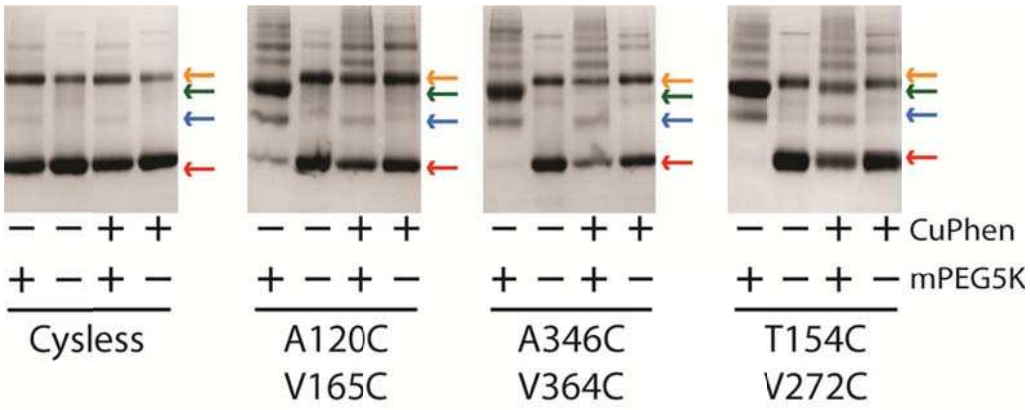


**Supplementary Figure 4. Chemical crosslinking with CuPhen protects outward-stabilizing cysteine pairs from mPEG5K labeling.** SDS-PAGE band-shift assay showing the number of free cysteines present in Cysless and the three double cysteine mutants; A120C/V165C, T154C/V272C, and A346C/V364C, with (+) and without (-) prior treatment with CuPhen. The following protein species seen in the gels are indicated by colored arrows; unmodified VcINDY (*red arrow*), dimeric VcINDY (*orange arrow*), singly PEGylated VcINDY (*blue arrow*), and doubly PEGylated VcINDY (*green arrow*).

**Supplementary Figure 5**

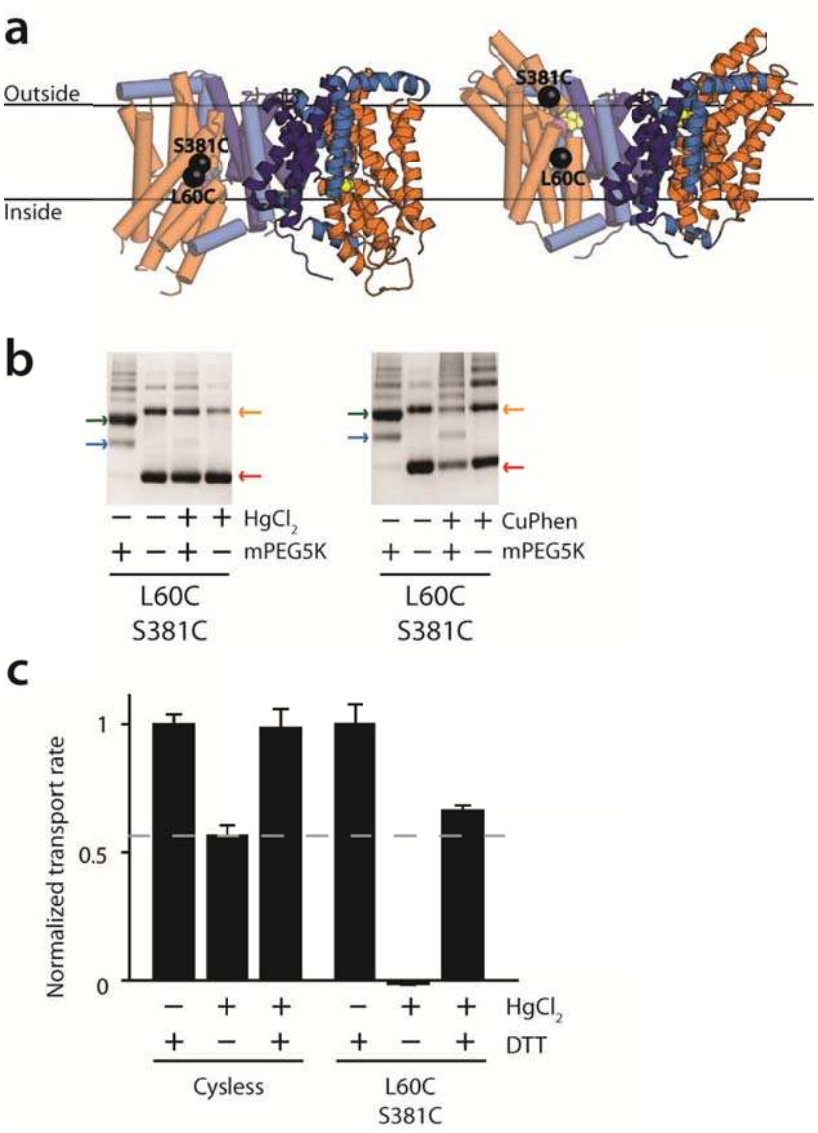


**Supplementary Figure 5. Inward-stabilizing crosslinks abolish transport activity of VcINDY.**

**(a)** Cartoon representation of the dimeric VcINDY inward-facing crystal structure (*left*) and the outward-facing model (*right*) viewed from the membrane plane. Substrates (citrate and $Na^+$) are shown as yellow and pink spheres. Cα-atoms of the inward-stabilizing residues are shown as black spheres (*left-hand side protomers*). **(b)** SDS-PAGE band-shift assay showing the number of free cysteines present in L60C/S381C with (+) and without (-) prior treatment with $HgCl_2$ (*left panel*) or CuPhen (*right panel*). The following protein species seen in the gels are indicated by colored arrows; unmodified VcINDY (*red arrow*), dimeric VcINDY (*orange*), singly PEGylated VcINDY (*blue*), and doubly PEGylated VcINDY (*green*). **(c)** Normalized initial rates of [$^3$H]-succinate transport in the presence of proteoliposomes containing Cysless and

L60C/S381C mutant after treatment with (+) and without (-) $HgCl_2$ and DTT. Results from triplicate datasets are shown and error bars represent S.E.M.

**Supplementary Figure 6**

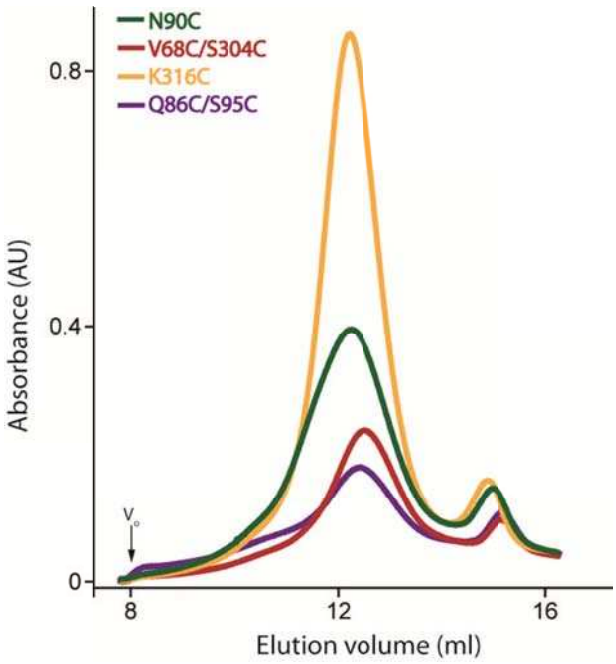


**Supplementary Figure 6. Dimer interface cysteine mutants are stable in detergent.** Size exclusion chromatography (SEC) traces showing the absorbance at $A_{280}$ for the four dimer interface cysteine mutants; N90C (*green*), V68C/S304C (*red*), K316C (*yellow*), and Q86C/S95C (*blue*). $V_0$ is ~8 ml and VcINDY elution peak is centered on 12.5 ml on the S200 SEC column.

**Supplementary Figure 7**

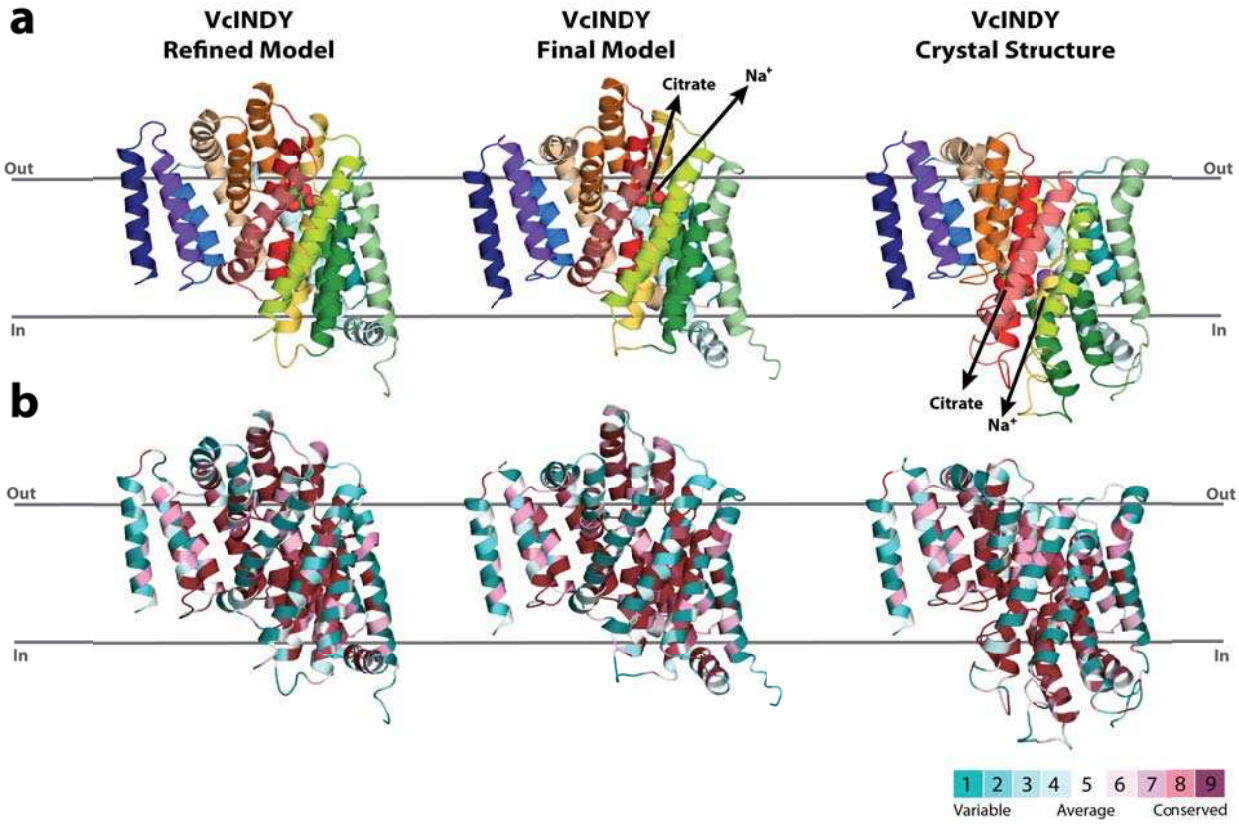


**Supplementary Figure 7. Comparison of the models generated with and without intradomain restraints with the VcINDY X-ray structure (PDB id: 4F35). (a)** Cartoon representation of the model obtained before applying distance restraints within the scaffold and transport domains ("refined model") and the model obtained after applying restraints ("final model") and the VcINDY structure used as template. Note that the alignment used to build both models is the same. The coloring scheme is that used in the transmembrane definition and the substrate and sodium ion are shown as green, red and purple spheres. **(b)** The coloring scheme reflects the conservation score for each residue obtained using the ConSurf server[43].